iScience

CellPress
OPEN ACCESS

Article

Hydrolytically stable foamed HKUST-1@CMC composites realize high-efficient separation of U(VI)

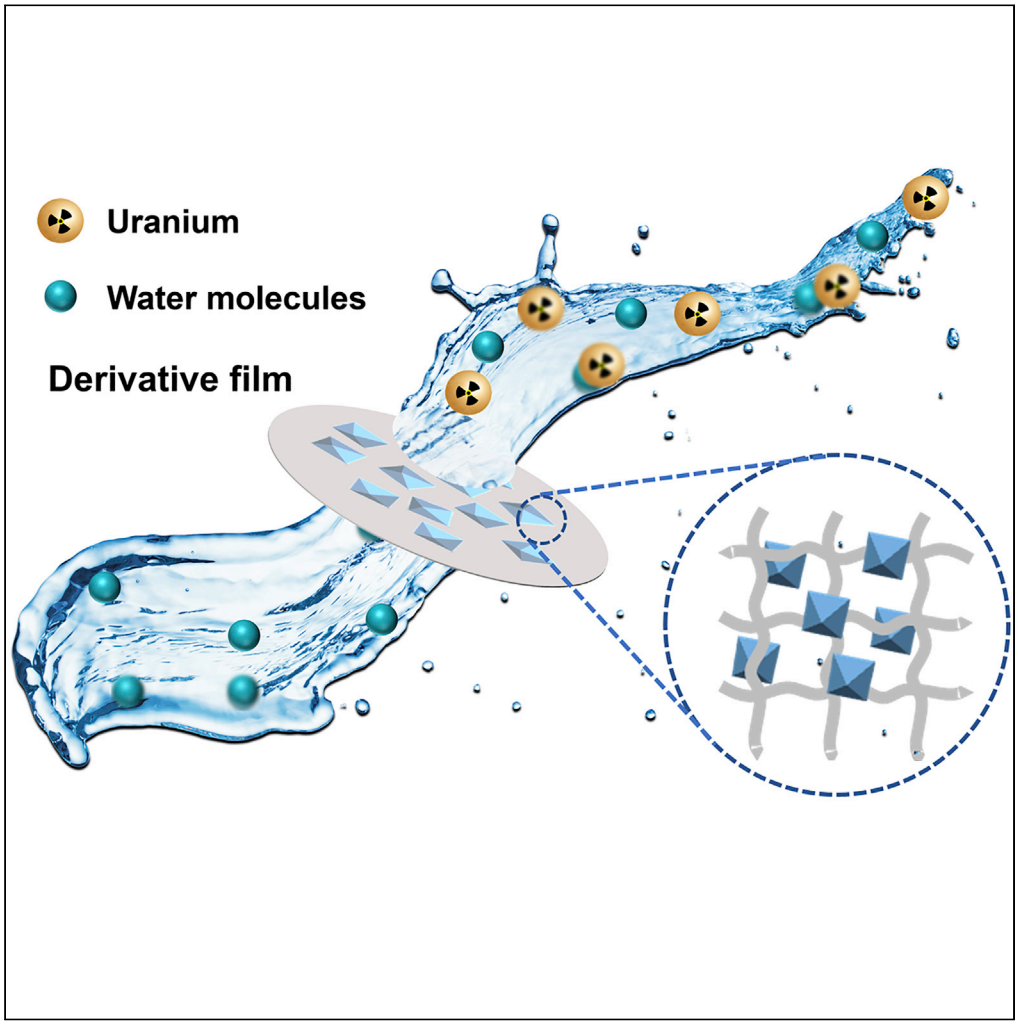

Dejun Zeng, Liyong Yuan, Pengcheng Zhang, ..., Youqun Wang, Yunhai Liu, Weiqun Shi

yuanly@ihep.ac.cn (L.Y.)
yhliu@ecut.edu.cn (Y.L.)
shiwq@ihep.ac.cn (W.S.)

Highlights

HKUST-1@CMC composites were obtained by using foaming strategy

HKUST-1@CMC composites show good acid and alkali resistance and radiation resistance

HKUST-1@CMC composites have high performance in U(VI) capture from aqueous solution

The derivative film was prepared, and the dynamic adsorption was conducted

Zeng et al., iScience 24, 102982
September 24, 2021
https://doi.org/10.1016/j.isci.2021.102982

iScience

CellPress
OPEN ACCESS

Article

Hydrolytically stable foamed HKUST-1@CMC composites realize high-efficient separation of U(VI)

Dejun Zeng,[1,2] Liyong Yuan,[1,*] Pengcheng Zhang,[3] Lin Wang,[1] Zijie Li,[1] Youqun Wang,[2] Yunhai Liu,[2,*] and Weiqun Shi[1,4,*]

SUMMARY

HKUST-1@CMC (HK@CMC) composites that show good acid and alkali resistance and radiation resistance were successfully synthesized by introducing carboxymethyl cellulose (CMC) onto the surface of HKUST-1 using a foaming strategy. For the first time, the composites were explored as efficient adsorbents for U(VI) trapping from aqueous solution, with encouraging results of large adsorption capacity, fast adsorption kinetics, and desirable selectivity toward U(VI) over a series of competing ions. More importantly, a hybrid derivative film was successfully prepared for the dynamic adsorption of U(VI). The results show that ~90% U(VI) can be removed when 45 mg L^{-1} U(VI) was passed through the film one time, and the removal percentage is still more than 80% even after four adsorption-desorption cycles, ranking one of the most practical U(VI) scavengers. This work offers new clues for application of the Metal-organic-framework-based materials in the separation of radionuclides from wastewater.

INTRODUCTION

With the depletion of traditional fossil energy, the energy crisis is sweeping the world (Xiong et al., 2020; Tang et al., 2020). Nuclear energy features cleanliness, high efficiency, and low carbon and thus is considered to be one of the most promising energy sources (Wang et al., 2020). Uranium is the most common nuclear fuel, uranium-containing wastewater runs through the entire nuclear energy utilization process, and a series of environmental problems caused by it have attracted increasing attention (Flett et al., 2021). In addition, from the point of improving the utilization of uranium resources, the separation and enrichment of U(VI) from wastewater are of great practical significance (Zou et al., 2020). Plenty of studies have shown that adsorption has the advantages of high efficiency, low cost, and simple operation, and it is currently one of the most common and effective methods for separating and enriching U(VI) from water samples (Dai et al., 2020; Wang et al., 2016; Zhu et al., 2017).

Metal-organic-frameworks (MOFs) are recently well known as a kind of porous coordination polymer, with the advantages of large specific surface area, adjustable pore size, and easy modification (Ding et al., 2019; Mei et al., 2019). They have shown attractive opportunities in the field of radionuclide adsorption and separation. Wang *et al.*, for example, synthesized a rod-like MOF-5 by the solvothermal method with extremely high affinity for U(VI), and the adsorption reaches equilibrium within 5 min (Wu et al., 2018). Sun *et al.* reported the first case of Tb-MOF-76 that can be used for both luminescence sensing and U(VI) adsorption, providing a candidate for simultaneous monitoring and separation of radionuclides related to nuclear fuel (Yang et al., 2013). Luo *et al.* proposed for the first time an anion-exchange strategy based on cation MOFs, which can directly extract U(VI) from alkaline solution and seawater (South China Sea) (Li et al., 2017). We recently prepared amino derivatives of MIL-101 by grafting strategy, which feature acid resistance and high activity, and thus can be used for U(VI) capture from acid solution (Bai et al., 2015). All these works clearly demonstrate the vast potential of MOFs applied in the radionuclide separation.

However, plenty of works have also shown that owing to the relatively low strength of the metal coordination bond, the framework of MOFs is easy to collapse in the aqueous solution, thus causing the decomposition of materials (Álvarez et al., 2017). Therefore, the hydrostability of MOFs is a key factor determining their application. People have tried several methods to improve the hydrostability of MOFs, among which

[1]Laboratory of Nuclear Energy Chemistry, Institute of High Energy Physics, Chinese Academy of Sciences, Beijing 100049, China

[2]State Key Laboratory of Nuclear Resources and Environment, East China University of Technology, Nanchang 330013, Jiangxi, China

[3]Engineering Laboratory of Advanced Energy Materials, Ningbo Institute of Industrial Technology, Chinese Academy of Sciences, Ningbo, Zhejiang 315201, China

[4]Lead contact

*Correspondence: yuanly@ihep.ac.cn (L.Y.), yhliu@ecut.edu.cn (Y.L.), shiwq@ihep.ac.cn (W.S.)

https://doi.org/10.1016/j.isci.2021.102982

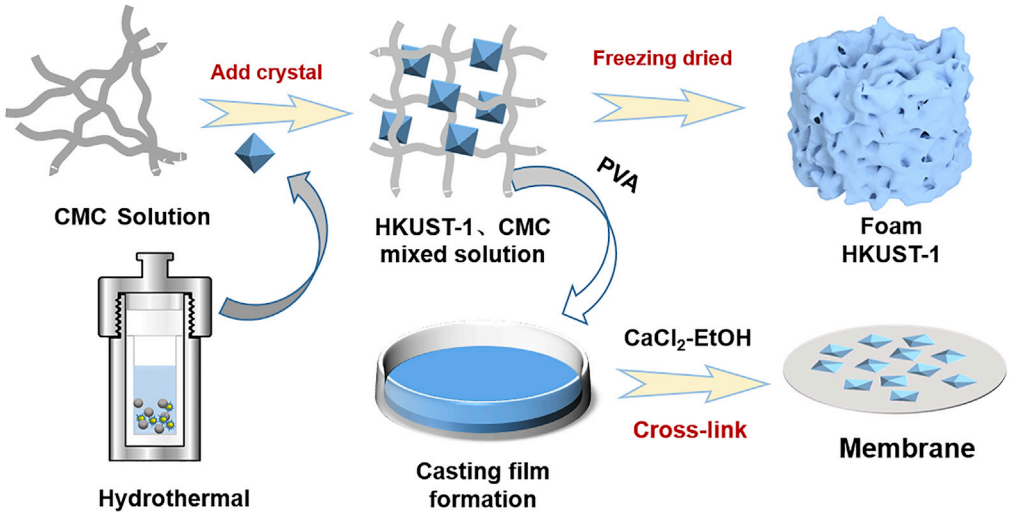

Figure 1. Synthetic schematic diagram of the HK@CMC composites and its derivative film

compounding with an inert matrix represents the most effective strategy (Jasuja et al., 2012). Matzger *et al.*, for example, successfully synthesized an MOF-5-based composite with styrene by initiator-free polymerization, and the composite remained stable in humid air (relative humidity [RH] = 53%) for 3 months (Gamage et al., 2016). Loh *et al.* designed a graphene oxide (rGO)/Cu-MOF hybrid composite by using the heterogeneity of porous scaffold structure and the synergistic effect between rGO and MOF. It is found that the composite still shows high activity for hydrogen evolution reaction (HER) and is stable even in 0.5 mol L^{-1} H_2SO_4 (Jahan et al., 2013). Sun *et al.* took the mesoporous structure of SBA-15 as a protective layer and encapsulated MOF-5 in the channel of SBA-15 using a dual-solvent strategy, which significantly improved the hydrostability of MOF-5 (e.g., it is well preserved after 8 h of exposure to a humid environment) (Kou and Sun 2018).

In addition to stability, another factor that limits the practical application of MOFs is its powder nature. As a kind of powder crystals, MOFs can be readily broken down into tiny particles during their separation, catalysis, and other industrial applications, which can easily block reactors and pipelines (Chen et al., 2016a, 2016b; Kalaj et al., 2020). Furthermore, the tiny particles always cause serious material loss and huge waste, which is also harmful to the practical application of MOFs. Compounding MOFs with suitable binders or additives to form uniform particles, membranes, textiles or fibers is one of the most effective strategies to overcome the aforementioned problems, before which choosing a suitable adhesive is necessary and important (Czaja et al., 2009). Carboxymethyl cellulose (CMC) is an important derivative of cellulose, which is widely used in various biomedical membranes owing to its extensive sources, nontoxic and tasteless nature, excellent film-forming and emulsifying properties, good biodegradability, and compatibility (Han et al., 2013). Besides, CMC contains a lot of hydroxyl (-OH) and carboxyl (-COOH), which can chelate with heavy-metal ions or dyes in wastewater to achieve high efficiency in water purification (Astrini et al., 2015; Hu et al., 2016).

In this work, using HKUST-1 (Cu node) as the base MOFs, a series of HK@CMC composites with different mass ratios were synthesized through a foaming strategy (Figure 1). And the hydrostability of the composites and its adsorption performance for U(VI) were studied in detail. The results shows that the hydrostability of the composites was significantly improved while the adsorption capacity for U(VI) was not significantly reduced. Moreover, the HK@CMC derivative film was synthesized through the strategy of casting film formation, and the reusability of the film was evaluated by dynamic separation experiments. This work provides a new strategy for improving the application feasibility of MOFs in an aqueous environment.

RESULTS

Structural characterizations

To verify that the target materials were successfully prepared, all the composites as well as HKUST-1 were fully characterized. The scanning electron microscopy (SEM) image (Figure S2) of the composite shows that the HKUST-1 powder after the foaming process was bonded together by the polymer CMC. The surface of

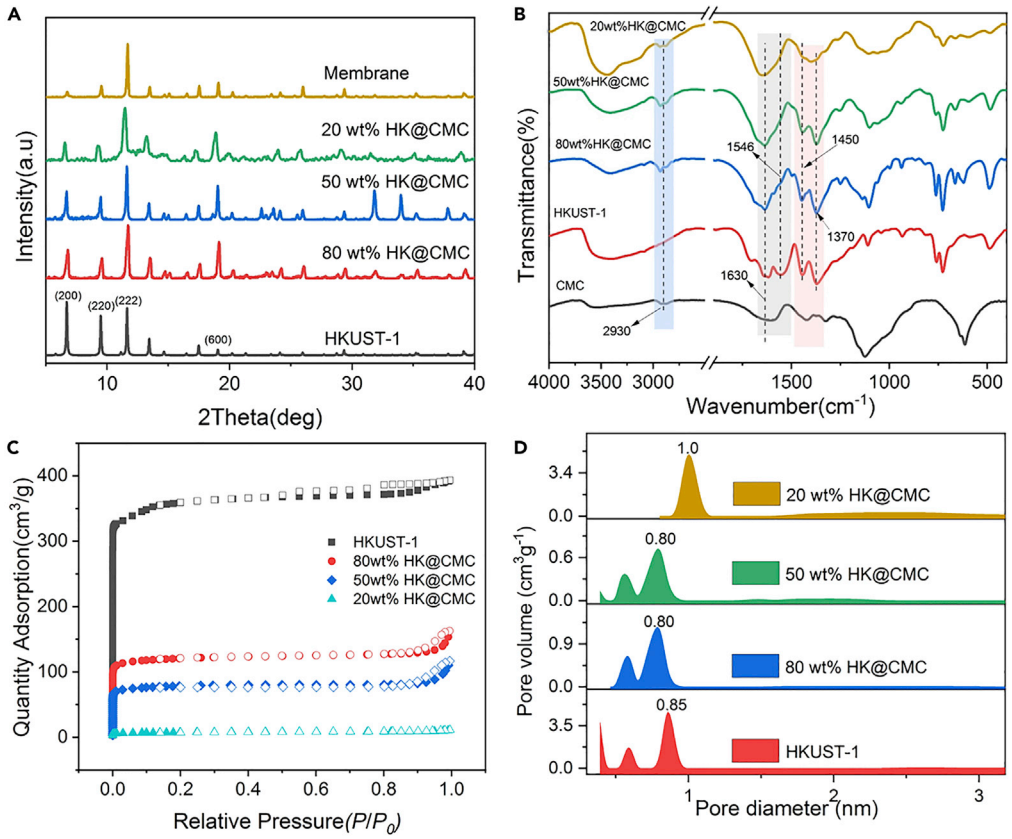

Figure 2. Structural characterizations of the prepared HK@CMC samples

(A) PXRD.

(B) FT-IR spectrum.

(C) N_2 adsorption-desorption isotherms.

(D) Pore size distribution.

HKUST-1 was attached to the CMC fragments, and as the proportion of CMC increased to 80 wt% (i.e., 20 wt% HK@CMC), the surface of HKUST-1 was almost completely covered by CMC. But on the whole, HKUST-1 retains the regular octahedral structure. The powder X-ray diffraction (PXRD) patterns of the composites (Figure 2A) were consistent with those of the simulated HKUST-1. All the diffraction peaks are sharp and strong, indicating that HKUST-1 not only maintains its original structure in the composites but also maintains a high degree of crystallinity. As HKUST-1 is wrapped and covered by amorphous CMC (Figure S3), the peak intensities of the lattice plane (200) and (220) of HKUST-1 in the composites were reduced, while the lattice plane (600) sharply enhanced. At the same time, with the increase of the CMC ratio (such as 20 wt % HK@CMC), the diffraction peaks of the composites broadened slightly, indicating that the crystallinity of the composites is slightly reduced. The PXRD results confirm that the target materials were successfully prepared, and the existence of CMC does not change the lattice structure of HKUST-1. Figure 2B compares the Fourier-transform infrared (FT-IR) spectra of the composites with different mass ratios. As can be seen, all the composites exhibit the characteristic peaks of HKUST-1. The relatively strong peaks at 3,420 cm^{-1} and 1,630 cm^{-1} can be attributed to the tensile vibration peaks of -OH and $-COO^{-}$, respectively (Tang et al., 2011; Xiao et al., 2018). The characteristic peak at 2,930 cm^{-1} is the asymmetric extension peak of $-CH_2$ in the hydroxymethyl (R-CH_2OH) moiety on CMC (Takigami et al., 2007), which indicates that the composite composed of HKUST-1 and CMC was successfully prepared. At the same time, the incorporation of CMC also has effects on the characteristic peaks of HKUST-1. For instance, the bending vibration peaks at 1,630 cm^{-1}/1,546 cm^{-1} and the characteristic peaks at 1,450 cm^{-1}/1,370 cm^{-1} were symmetrical distributed on HKUST-1. However, with the introduction of CMC, the two peaks became asymmetric (Back et al., 2017; Cui et al., 2019). Especially in 20 wt% HK@CMC, these four peaks turned into two broad characteristic peaks. This may result from the formation of the hydrogen bond between -OH in CMC and -COOH in

Table 1. Specific surface area and total pore volume of pristine HKUST-1 and HK@CMC composites

Materials	Brunner-Emmet-Teller (BET) surface area ($m^2\ g^{-1}$)	Pore volume ($m^3\ g^{-1}$)
HKUST-1	1217	0.60
80 wt% HK@CMC	407	0.22
50 wt% HK@CMC	265	0.15
20 wt% HK@CMC	26	0.02

HKUST-1 (Li et al., 2018, 2020). Moreover, by comparing the infrared spectra of the derivative film and CMC, we found that compared with CMC, the absorption of the O-H bond of the derivative film shifted to a lower wavenumber (from 3,570 cm^{-1} to 3,400 cm^{-1}) (Figure S4). This is because the hydroxyl and carboxyl groups on the CMC are chelated and coordinated with Ca^{2+}, which reduces the hydrogen bond interaction between the hydroxyl functional groups (Che Nan et al., 2019). This result indicates that Ca^{2+} successfully formed intramolecular and intermolecular bonds with CMC to achieve chemical cross-linking. The N_2 adsorption-desorption curves of the composites were determined, and the results are shown in Figure 2C. It can be seen that the composites exhibit a typical type I adsorption isotherm, showing a microporous structure. Pristine HKUST-1 shows a specific surface area as high as 1,217 $m^2\ g^{-1}$. With the existence of CMC and the decrease of the proportion of HKUST-1 in the composites (from 80 wt% to 20 wt%), however, the specific surface area of the composites gradually decreases from 407 $m^2\ g^{-1}$ to 26 $m^2\ g^{-1}$. This is mainly because CMC and HKUST-1 are composited on the surface, making the polymer CMC fragments become a part of HKUST-1, so the specific surface area and pore volume of the composite are inevitably reduced, which is consistent with some other MOF@polymer reports (Huo et al., 2013; Fu et al., 2017). The pore size was obtained from the max of the pore size distribution curve calculated by the Barrett-Joyner-Halenda (BJH) method using the adsorption branch of the isotherm. The total pore volume was evaluated by the single point method. The results are shown in Figure 2D and Table 1. As can be seen, although the introduction of CMC has caused a significant decrease in the specific surface area and pore volume of the composites, the pore size has not changed significantly.

Stability examination

Thermogravimetric analysis (TGA) was used to characterize the thermal stability of the composites, and the results are shown in Figure 3A. It can be clearly seen that the decomposition temperatures of HKUST-1 and CMC are 335°C and 256°C, which are caused by skeleton collapse and decarboxylation, respectively (Biswal and Singh 2004). 80wt% HK@CMC shows the similar weight loss process with pristine HKUST-1 (Fu et al., 2017), denoting the dominant species of HKUST-1 in this composite. However, 50 wt% HK@CMC and 20 wt% HK@CMC had two weight loss processes, which were caused by decarboxylation and decomposition of residual carbonates, respectively (Saadiah et al., 2019). From the differential thermogravimetric (DTG) curve (Figure S5), it can be seen that as the mass ratio of HKUST-1 in the composites increases from 20 wt% to 80 wt%, the decomposition temperature of the composites increases from 205°C to 279°C, which seems to give a hint that increasing the content of HKUST-1 in the composite is beneficial to improve the thermal stability of the composite.

Hydrostability is one of the most important properties of MOF science. In many cases, it is unavoidable to handle MOF samples in water. In order to measure the hydrostability of the composites, a certain amount of samples was dispersed in deionized water and stirred for different times. The PXRD patterns of the processed sample were then recorded. The results are shown in Figure 3B. It can be seen that HKUST-1 has new diffraction peaks at $2\theta = 9.9°$ and 11° after stirring for 40 min, indicating that the framework has begun to collapse at this time (Figure S6A). The collapse of 80 wt% HK@CMC is much slower than that of HKUST-1. It can remain stable for 180 min in water, and the new diffraction peak appears only at 240 min (Figure S6B). For 50 wt% HK@CMC, no new or disappearing peaks are observed even after 720 min, which indicates a higher hydrostability (Figure S6C). Furthermore, considering the various harsh conditions such as high acidity and radiation of the radioactive wastewater, the adsorbent should be kept stable under these conditions. We thus measured the stability of HKUST-1, 80 wt% HK@CMC, and 50 wt% HK@CMC in the pH range of 2.0–11.0, in which a certain amount of adsorbent was stirred in aqueous solutions with different pH for 30 min (Figure 3C). It can be seen that the skeleton of HKUST-1 powder begins to collapse under near-neutral (pH 6.0 and 8.0) conditions, while the skeletons of 80 wt% HK@CMC and 50 wt% HK@CMC were

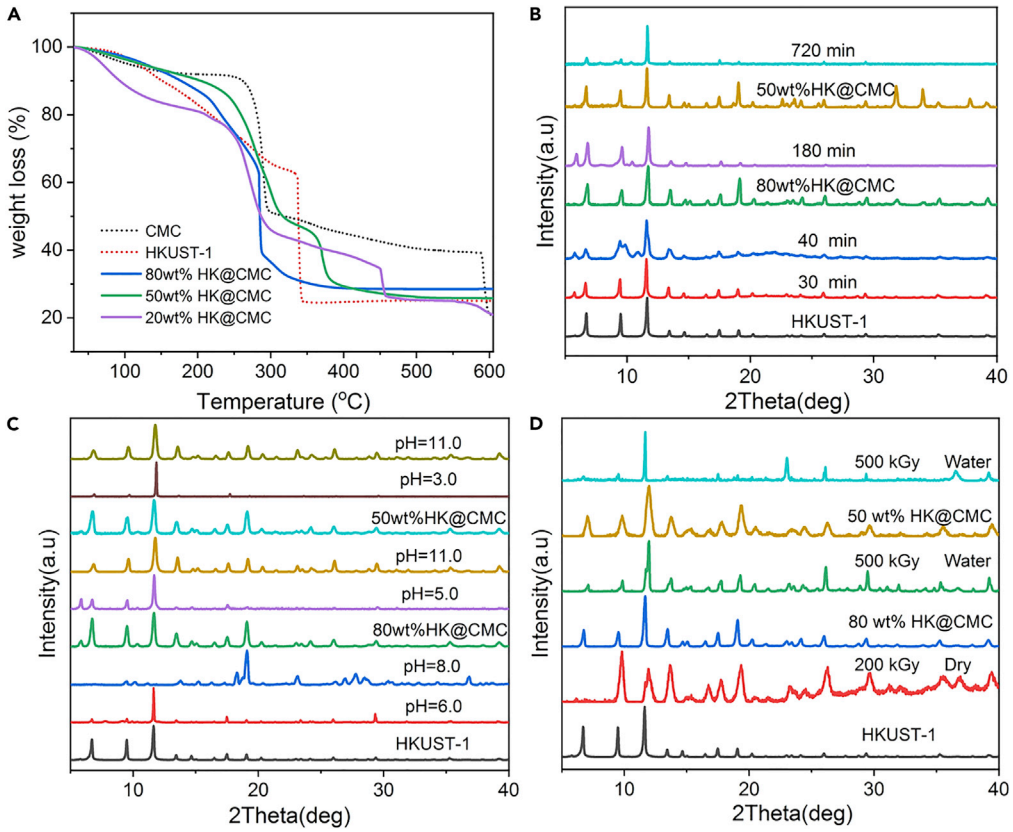

Figure 3. Stability examination of the prepared HK@CMC samples

(A) TGA curves of as synthesized composites.

(B) Hydrostability.

(C) Stability at different pH values.

(D) Radiation stability.

kept stable in the range of pH 5.0–11.0 and pH 3.0–11.0, respectively, showing good acid-base stability of the composites (Figure S7). At the same time, we also carried out the irradiation experiment, in which the dried composites and the composites immersed in water were irradiated under ^{60}Co (γ irradiation), respectively, and the irradiation doses were 200 kGy and 500 kGy (Figure S8). As can be seen, the skeleton of HKUST-1 has been decomposed at a dose of 200 kGy, whereas even if immersed in water, the skeletons of 80 wt% HK@CMC and 50 wt% HK@CMC can be well maintained under the irradiation dose of up to 500 kGy, indicating that the composites have excellent radiation stability (Figure 3D). These results show that the stability (including hydrostability, acid-base stability, and radiation stability) of HKSUT-1 after foaming has been greatly improved, and it is suitable for capturing radionuclides from wastewater.

Batch adsorption of U(VI)

Effect of pH

The solution pH often plays an important role during the adsorption and separation of metal ions. It not only affects the surface potential of adsorbent but also affects the species of metal ions in the solution (Han et al., 2019; Yuan et al., 2020). Therefore, the U(VI) adsorption by the composites (i.e., 80 wt% HK@CMC, 50 wt% HK@CMC and 20 wt% HK@CMC) and CMC for in the pH range of 2.0–4.5 was studied, and the results are shown in Figure 4A. It is clear that the U(VI) adsorption in all the materials is pH dependent. That is, all the materials have no obvious adsorption for U(VI) at pH 2.0. As the pH increases to 4.5, the adsorption capacity of U(VI) on CMC, 20 wt% HK@CMC, 50 wt% HK@CMC, and 80 wt% HK@CMC gradually increased to 186 mg g^{-1}, 256 mg g^{-1}, 291 mg g^{-1}, and 344 mg g^{-1}, respectively. The zeta potential of the adsorbents can explain this pH-dependent adsorption process. When the pH value is low, a large amount of H^+ (H_3O^+) in the solution protonates the functional groups of the adsorbent and occupies the active sites

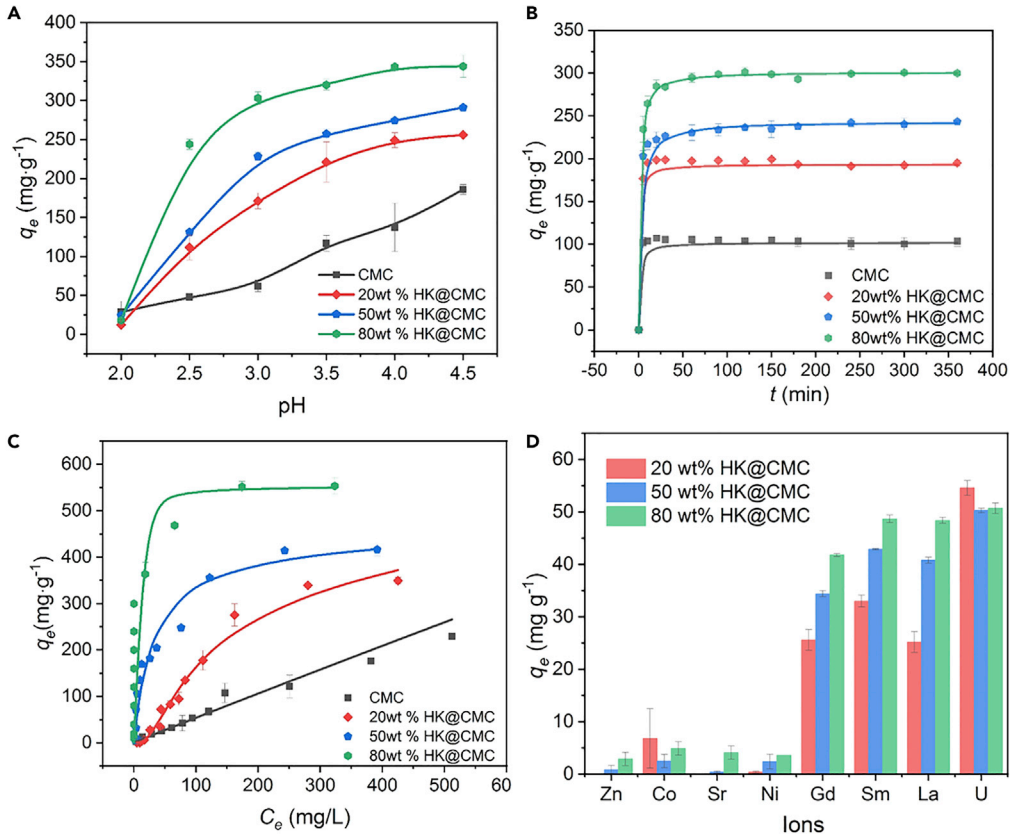

Figure 4. The adsorption behavior of U(VI) in the three composites and CMC under different conditions.

$m_{adsorbent}/V_{solution}$ = 0.5 mg mL^{-1}

(A) pH dependence ($[U]_{initial}$ = 200 mg L^{-1}, t = 360 min).

(B) Adsorption kinetics (pH = 3.0 ± 0.1, $[U]_{initial}$ = 200 mg L^{-1}, and the solid line represents the fitted kinetic curve).

(C) Adsorption isotherm (pH = 3.0 ± 0.1, t = 360 min, and the solid line represents isotherm fitting).

(D) The effect of competitive ions on the adsorption (pH = 3.0 ± 0.1, $[Ions]_{initial}$ = 50 mg L^{-1}, t = 360 min).

on the surface of the adsorbent, thus leading to a low U(VI) adsorption. As the pH increases to 4.5, the zeta potential of HKUST-1 decreases from 4.5 mV to −5.6 mV, while the introduction of CMC makes the composites exhibit a more negative overall potential (Figure S9A). Meanwhile, U(VI) species gradually changed from free UO_2^{2+} to polynuclear hydroxide complexes (Figure S9B) (such as $(UO_2)_2(OH)_2^{2+}$ and $(UO_2)_3(OH)_5^{+}$). These polynuclear hydroxides are more easily adsorbed by the negative adsorbents, thus leading to an increase in U(VI) absorption (Zhang et al., 2017; Yuan et al., 2011).

Adsorption kinetics

By changing the contact time from 5 min to 360 min, the adsorption kinetics of U(VI) on 80 wt% HK@CMC, 50 wt% HK@CMC, 20 wt% HK@CMC, and CMC were studied. The results are listed in Figure 4B. It can be seen that in the first 10 min, the U(VI) adsorption in all the increases rapidly. Especially as the proportion of CMC in the composites increases, the adsorption rate increases faster. The U(VI) adsorption in 20 wt% HK@CMC and CMC, for example, is close to equilibrium at ~10 min, while for 80 wt% HK@CMC and 50 wt% HK@CMC, a dynamic equilibrium was reached at 30 min. Such a result can be rationalized as follows: U(VI) is first chelated with the exposed -COO- group on CMC which is located on the surface of the composites and then trapped. When the adsorption site on CMC was occupied, U(VI) coordinates with the abundant oxygen atoms on HKUST-1. In order to clarify the adsorption process, the pseudo-first-order and the pseudo-second-order kinetic models were applied to fit the experimental data (Figure S10), and the model parameters obtained by the both models are shown in Table S1. Obviously, the adsorption data for all the composites can be well fitted by the pseudo-second-order kinetic model, and the linear correlation (R^2) of the fitting was more than 0.99 (Figure S10 and Table S1). In other words, the pseudo-second-order kinetics is more suitable for describing these adsorption processes, indicating a chemical adsorption.

Table 2. Comparison of various adsorbents for U(VI) ion adsorption

Adsorbent	Experimental conditions	Equilibration time (min)	q_{max} (mg g^{-1})	References
Nanoring(NNRG)	pH = 4.0	60	265	Kushwaha et al. (2020)
ImP(O) $(OH)_2/SiO_2$	pH = 4.0	120	618	Budnyak et al. (2018)
polyacrylic acid (PAA)/CS	pH = 4.0	250	289.6	He et al. (2018)
Poly (acrylic acid-co-acrylamide)(PAAAM)	pH = 4.0	300	713.2	Wei et al. (2018)
PAA hydrogel	pH = 4.0	120	445.1	Yi et al. (2017)
Y-MOF-76	pH = 3.0 ± 0.1	300	298	Yang et al. (2013)
UiO-68-P(O) $(OEt)_2$	pH = 2.5	–	217	Carboni et al. (2013)
80 wt% HK@CMC	pH = 3.0 ± 0.1	30	550	This work

Adsorption isotherm

Keeping the solid-liquid ratio constant, the saturation adsorption capacity of the composites for U(VI) was determined by changing the concentration of U(VI) in the solution at pH 3.0. The results are shown in Figure 4C. It is clear that as the concentration of U(VI) increases, the U(VI) adsorption in all the composites increases. Especially as the initial concentration of U(VI) increases from 10 mg L^{-1} to 200 mg L^{-1}, the U(VI) adsorption on the three composites all sharply increase. As the U(VI) concentration continues to increase to 600 mg L^{-1}, the amount of U(VI) adsorbed by the composites hardly increases. At this time, the saturated adsorption capacities of 80 wt% HK@CMC, 50 wt% HK@CMC, and 20 wt% HK@CMC were calculated to be 550 mg g^{-1}, 416 mg g^{-1} and 349 mg g^{-1}, respectively. Such an adsorption isotherm is understandable because the increase of U(VI) concentration causes the change of the concentration gradient of solid and liquid phases, thereby leading to the increase of the driving force of the adsorption process. When the adsorption sites are completely occupied, the adsorption amount no longer increases. It is worth noting that although the composition of these composite is completely the same except for the difference in the proportion of HKUST-1, the U(VI) adsorption in them is significantly different from each other, which indicates that HKUST-1 plays a major role in the adsorption of U(VI). The Langmuir and Freundlich models were used to analyze the adsorption mode of U(VI) on these adsorbents (Figure S11), and the model parameters obtained by both the models are shown in Table S2. As can be seen that when the proportion of HKUST-1 is dominant in the composites (e.g., 80 wt% HK@CMC and 50 wt% HK@CMC), the adsorption process is more consistent with the Langmuir model ($R^2 \geq 0.99$), and the theoretical adsorption capacities ($q_{e,cal}$, 552 mg g^{-1} and 452 mg g^{-1}) obtained by the Langmuir adsorption model are close to the experimental values ($q_{e,exp}$, 553 mg g^{-1} and 417 mg g^{-1}), which indicates that the adsorption of U(VI) in these two composites is a monolayer adsorption, whereas for 20 wt% HK@CMC and CMC, the Freundlich model gave a better fit ($R^2 \geq 0.87$), which suggests that the adsorption of U(VI) in these two materials is multilayer adsorption.

In addition, we compared the synthesized HK@CMC composite with some other U(VI) adsorbents in the range of pH 2.0–4.0, and the results are listed in the Table 2. Although it is a bit far-fetched to directly compare the HK@CMC composite with these reported adsorbents owing to the different experimental conditions such as the solid-liquid ratio in the batch experiment, it can still be seen that the adsorption capacity of 80 wt% HK@CMC for U(VI) is in the forefront. At the same time, the time required for adsorption equilibrium is the shortest, indicating that the materials in this work are efficient U(VI) capture agents.

Selectivity test

The composition of radioactive wastewater is complex, which generally includes various transition metal elements and lanthanides with charges ranging from ^{30}Zn to ^{71}Lu. Thus, the selective adsorption capacity of a material is an important criterion for its practical application. Herein, we carried out competitive adsorption experiments to evaluate the selectivity of the composites by choosing seven coexisting ions including Zn(II), Co(II), Sr(II), Ni(II), Gd(III), Sm(III), and La(III) (Ouyang et al., 2020). The adsorption was carried out at a constant pH of 3.0, and the concentration of each ion is identical to 50 mg L^{-1}. The results are shown in Figure 4D. It is found that even in the presence of high concentrations of these competing ions, all the composites still remain high affinity for U(VI) with the adsorption capacity of more than 50 mg g^{-1},

whereas for the divalent transition metal ions such as Zn(II) and Co(II), the values are all lower than 10 mg g^{-1}. By calculating the distribution coefficient (K_d) and selectivity coefficient (S) (Table S3), we find that the K_d value for U(VI) is greater than 2000, while the S values for U(VI) over all the divalent transition metal ions are more than 15, which clearly indicates that these composites have a much higher affinity for U(VI) over divalent transition metal ions. The selectivity can be rationalized based on coordination and electrostatic interaction. HKUST-1 is formed by the coordination of 1,3,5-benzentricarboxylate (BTC) ligand with Cu(II), and each BTC ligand contains three carboxyl groups. These carboxyl groups contain a large number of oxygen atoms, which provide coordination sites for U(VI), so U(VI) is mainly adsorbed by the -COOH chelating effect (Liu et al., 2020; Lv et al., 2019). Compared with divalent metal ions such as Co(II) and Ni(II), U(VI) is a stronger Lewis acid and thus has a higher affinity with hard oxygen donors such as carboxyl groups (Yang et al., 2019). Li *et al.* also found through molecular dynamics simulation combined with density functional theory calculations that a carbonyl oxygen on the carboxyl group is coordinated to the center U(VI) in a monodentate manner (Li et al., 2016). In addition, Feng *et al.* found that HKUST-1 adsorption process of U(VI) involved not only chelating coordination but also coulomb electrostatic force (Feng et al., 2013). The effective charge of uranyl (the main form of U(VI)) is higher than divalent, thus leading to the selectivity of the composites toward U(VI) over divalent metal ions. Besides U(VI), the composite also showed a high adsorption capacity for trivalent ions, i.e., Gd(III), Co(III), and Sm(III) (Figure 4D), which is in line with the electrostatic-force-based mechanism.

Dynamic adsorption and reusability assessment

The high adsorption capacity and affinity of HK@CMC composites for U(VI) in static batch experiments prompted us to try to prepare a two-dimensional (2D) derivative film to achieve dynamic separation of U(VI). CMC has an excellent film-forming ability, but the formed film is often rigid and fragile after loss of water (Saadiah et al., 2019). Therefore, we introduced a little polyvinyl alcohol (PVA) into the mixed solution to construct a composite polymer system (HPe) and synthesized 75 wt% HK@CMC@PVA 2DM derivative films, where HKUST-1 accounts for 75 wt%, CMC accounts for 20 wt%, and PVA accounts for 5 wt%.

Before the dynamic separation experiment, we measured the mechanical properties of the film. The stress-strain curve is shown in Figure 5A, and the stress-strain parameters are listed in Table S4. The stress-strain curve of the film is nonlinear, which is similar to the tensile curve of flour, indicating that the introduction of PVA makes the film plastic. When the stress is 0–0.25 MPa, the film is in an elastic deformation stage and the elongation of film is 4% at this time. As the stress further increases to 0.31 MPa, the film is in the plastic deformation stage, and the elongation is ~3%. The tensile strength and elongation at the breakage of the derivative film are 0.31 MPa and 12.15%, respectively. The stress-strain curves show that the introduction of PVA greatly improves the mechanical properties of the film, thus guaranteeing the potential usage of the film in dynamic adsorption. In addition, as can be seen from SEM (Figure 5B), HKUST-1 maintains intact regular octahedral structure and is uniformly embedded in CMC. By measuring the cross section of the derived film (Nano Measure1.2), it is found that the thickness is *ca.* 140 μm. All these results further proved the feasibility of the film formation strategy.

The dynamic separation experiment was then carried out in the vacuum pumping filter device (Figure S1). In order to reduce the production of radioactive waste liquid, we used 5 mL of U(VI) (C_0 = 10 mg L^{-1}) for the separation experiment. It is found that the removal percentage of U(VI) by the film is higher than 90% in a wide pH range (2.0–4.5), and when the pH is greater than 3.5, the removal percentage is greater than 99% (Figure S12A). Moreover, even if the concentration of U(VI) is increased from 5 mg L^{-1} to 45 mg L^{-1}, the removal percentage of the film is still as high as ~90%, showing an excellent removal effect (Figure 5C). It is well known that the reproducibility and reusability of a solid material are important factors determining its potential in practical application. Given that the HK@CMC composites exhibit desirable hydrostability, the actual reusability of the film was tested. Specially, using 0.1 mol L^{-1} Na_2CO_3 as an eluent, we carried out consecutive adsorption and desorption experiments on the film. Before the cycle experiment, the elution percentages by different volumes of Na_2CO_3 were determined. It is found that when the volume of Na_2CO_3 increases from 5 mL to 20 mL, the elution percentage increase from 51% to 95% (Figure S12B), so the volume of the eluent was set to 20 mL. The results of the cycle experiments are shown in Figure 5D. It is found that even after four times of adsorption and desorption, the removal percentage of U(VI) by the film is still as high as 80%, demonstrating the excellent reusability of the film. In short, all these results highlight the enticing opportunities of the HK@CMC composites in dynamic adsorption of U(VI) and probably other radionuclides.

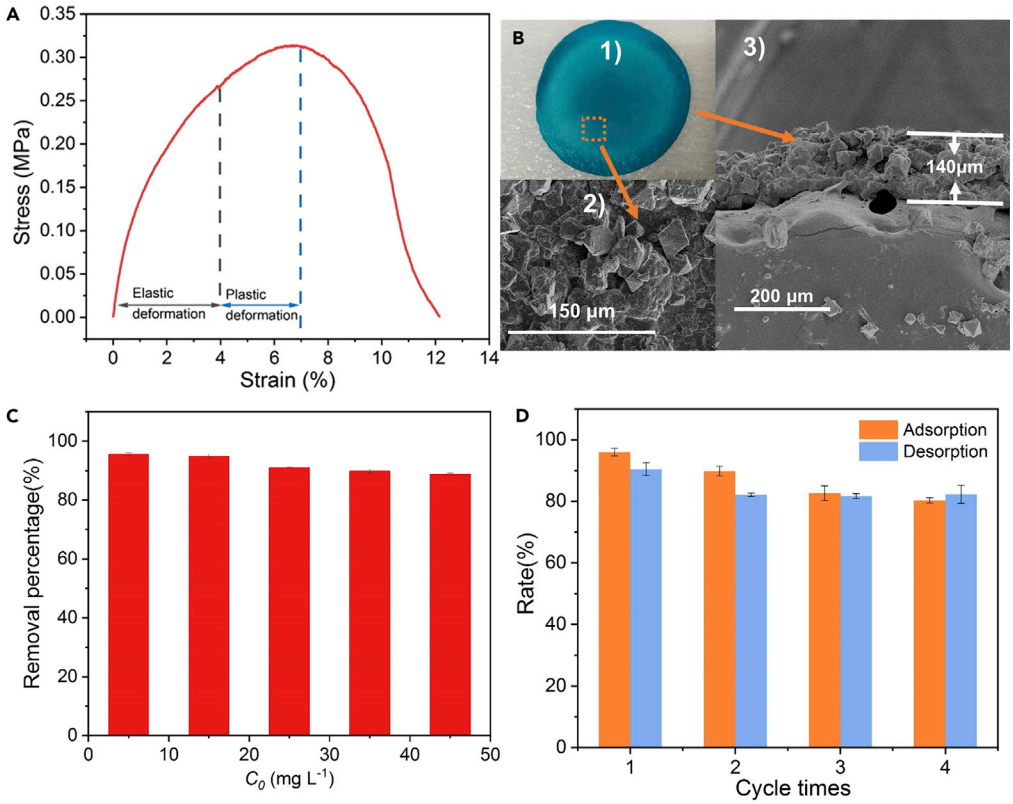

Figure 5. Characterizations of the derived film and its dynamic separation of U(VI)

(A) Stress-strain curve of the derivative film.

(B) Physical (above) and SEM (below) images of the film, and its SEM cross section image (right).

(C) The removal percentage for different concentrations of U(VI) on the derivative film.

(D) The removal percentage of U(VI) by the derivative film after multiple cycles (pH = 4.5 ± 0.1, $[U]_{initial}$ = 10 mg L^{-1}).

DISCUSSION

Although MOFs have recently been well documented as efficient adsorbents for separating U(VI), overcoming their poor hydrostability and improving their applicability still remain challenging. Herein, we incorporated CMC with HKUST-1 to fabricate a series of HK@CMC composites in different proportions through a foaming strategy. The batch adsorption of U(VI) in the composites was studied in detail. The derivative film was prepared by the casting film technology, and the reusability of the film was evaluated by dynamic separation experiments. Both the batch adsorption and dynamic separation experiments show that the HK@CMC composites are efficient and reusable U(VI) adsorbents. Meanwhile, the introduction of CMC greatly improves the stability (including hydrostability, acid-base stability, and radiation stability) of HKUST-1. While HKUST-1 begins to collapse after suspending in water for 40 min, the HK@CMC composite remains stable in water for more than 12 h, and the HKUST-1 crystal in the composite keeps intact even at pH 3.0 and pH 11.0. The performance of these materials suggests enticing opportunities in practical applications for removal of U(VI) as well as other radionuclides from the water environment, and liquid waste or process streams in spent nuclear fuel reprocessing.

Limitations of the study

This work synthesized the foamed HK@CMC composites, which provided a new strategy for the development and application of hydrostability MOFs in radionuclide separation. However, this study also has limitations. For example, we did not discuss the action path and mechanism of the foaming-based strategy to improve the hydrostability of HKUST-1. Furthermore, we only discussed that the foaming strategy has a significant effect on improving the hydrostability of HKUST-1, but whether this strategy also has such a significant effect on other MOFs with poor hydrostability (such as MOF-5) remains to be confirmed. That is, the universality of this strategy is not confirmed. Further works on these aspects are underway in our laboratory.

STAR★METHODS

Detailed methods are provided in the online version of this paper and include the following:

- KEY RESOURCES TABLE
- RESOURCE AVAILABILITY
  - Lead contact
  - Material availability
  - Data and code availability
- METHODS DETAILS
  - MOF synthesis
  - Composites synthesis
  - Preparation of derivative film
  - Static adsorption experiments
  - Dynamic adsorption experiments
  - The adsorption data fitting by kinetics models
  - The adsorption data fitting by isotherm models
  - Selective adsorption of U(VI) by the composites

SUPPLEMENTAL INFORMATION

Supplemental information can be found online at https://doi.org/10.1016/j.isci.2021.102982.

ACKNOWLEDGMENTS

This work was supported by the National Natural Science Foundation of China (Grants Nos. 21777161 and U20B2019) and the National Science Fund for Distinguished Young Scholars (No. 21925603). Youth Innovation Promotion Association of CAS (2017020) is also acknowledged.

AUTHOR CONTRIBUTIONS

Dejun Zeng: Methodology, Investigation, Formal analysis, Data Curation, Visualization, Writing - Original Draft; Liyong Yuan: Conceptualization, Writing - Review & Editing, Supervision, Funding acquisition; Pengcheng Zhang: Resources, Investigation; Lin Wang: Resources, Formal analysis; Zijie Li: Investigation, Formal analysis; Youqun Wang: Validation, Writing - Review & Editing; Yunhai Liu: Supervision, Funding acquisition; Weiqun Shi: Project administration, Funding acquisition; Writing - Review & Editing.

DECLARATION OF INTERESTS

The authors declare no competing interests.

Received: April 19, 2021
Revised: July 1, 2021
Accepted: August 10, 2021
Published: September 24, 2021

REFERENCES

Álvarez, J.R., Sánchez-González, E., Pérez, E., Schneider-Revueltas, E., Martínez, A., Tejeda-Cruz, A., Islas-Jácome, A., González-Zamora, E., and Ibarra, I.A. (2017). Structure stability of HKUST-1 towards water and ethanol and their effect on its CO_2 capture properties. Dalton T *46*, 9192–9200.

Astrini, N., Anah, L., and Haryadi, H.R. (2015). Adsorption of Heavy Metal Ion from Aqueous Solution by Using Cellulose Based Hydrogel Composite, Macromolecular Symposia (Wiley Online Library), pp. 191–197.

Back, S., Lim, J., Kim, N.-Y., Kim, Y.-H., and Jung, Y. (2017). Single-atom catalysts for CO_2 electroreduction with significant activity and selectivity improvements. Chem. Sci. *8*, 1090–1096.

Bai, Z.Q., Yuan, L.Y., Zhu, L., Liu, Z.R., Chu, S.Q., Zheng, L.R., Zhang, J., Chai, Z.F., and Shi, W.Q. (2015). Introduction of amino groups into acid-resistant MOFs for enhanced U (VI) sorption. J. Mater. Chem. A. *3*, 525–534.

Biswal, D., and Singh, R. (2004). Characterisation of carboxymethyl cellulose and polyacrylamide graft copolymer. Carbohyd Polym. *57*, 379–387.

Budnyak, T.M., Gładysz-Płaska, A., Strizhak, A.V., Sternik, D., Komarov, I.V., Majdan, M., and Tertykh, V.A. (2018). Imidazole-2yl-phosphonic acid derivative grafted onto mesoporous silica surface as a novel highly effective sorbent for uranium (VI) ion extraction. ACS Appl. Mater. Inter. *10*, 6681–6693.

Carboni, M., Abney, C.W., Liu, S., and Lin, W. (2013). Highly porous and stable metal–organic frameworks for uranium extraction. Chem. Sci. *4*, 2396–2402.

Che Nan, N.F., Zainuddin, N., and Ahmad, M. (2019). Preparation and swelling study of CMC hydrogel as potential superabsorbent. Pertanika J. Sci. Technol. *27*, 489–498.

Chen, Y., Huang, X., Zhang, S., Li, S., Cao, S., Pei, X., Zhou, J., Feng, X., and Wang, B. (2016a). Shaping of metal–organic frameworks: from fluid to shaped bodies and robust foams. J. Am. Chem. Soc. *138*, 10810–10813.

Chen, Y., Li, S., Pei, X., Zhou, J., Feng, X., Zhang, S., Cheng, Y., Li, H., Han, R., and Wang, B. (2016b). A solvent-free hot-pressing method for preparing metal–organic-framework coatings. Angew. Chem. Int. Edit *55*, 3419–3423.

Cui, X., Sun, X., Liu, L., Huang, Q., Yang, H., Chen, C., Nie, S., Zhao, Z., and Zhao, Z. (2019). In-situ fabrication of cellulose foam HKUST-1 and surface modification with polysaccharides for enhanced selective adsorption of toluene and acidic dipeptides. Chem. Eng. J. *369*, 898–907.

Czaja, A.U., Trukhan, N., and Müller, U. (2009). Industrial applications of metal–organic frameworks. Chem. Soc. Rev. *38*, 1284–1293.

Dai, Y., Lv, R., Fan, J., Peng, H., Zhang, Z., Cao, X., and Liu, Y. (2020). Highly ordered macroporous silica dioxide framework embedded with supramolecular as robust recognition agent for removal of cesium. J. Hazard Mater. *391*, 121467.

Ding, M., Cai, X., and Jiang, H.-L. (2019). Improving MOF stability: approaches and applications. Chem. Sci. *10*, 10209–10230.

Feng, Y., Jiang, H., Li, S., Wang, J., Jing, X., Wang, Y., and Chen, M. (2013). Metal–organic frameworks HKUST-1 for liquid-phase adsorption of uranium. Colloid Surf. A *431*, 87–92.

Flett, L., McLeod, C.L., McCarty, J.L., Shaulis, B.J., Fain, J.J., and Krekeler, M.P. (2021). Monitoring uranium mine pollution on Native American lands: insights from tree bark particulate matter on the Spokane Reservation, Washington, USA. Environ. Res. *194*, 110619.

Fu, Q., Wen, L., Zhang, L., Chen, X., Pun, D., Ahmed, A., Yang, Y., and Zhang, H. (2017). Preparation of ice-templated MOF–polymer composite monoliths and their application for wastewater treatment with high capacity and easy recycling. ACS Appl. Mater. Inter. *9*, 33979–33988.

Gamage, N.D.H., McDonald, K.A., and Matzger, A.J. (2016). MOF-5-Polystyrene: direct production from monomer, improved hydrolytic stability, and unique guest adsorption. Angew. Chem. Int. Edit *55*, 12099–12103.

Han, B., Zhang, D., Shao, Z., Kong, L., and Lv, S. (2013). Preparation and characterization of cellulose acetate/carboxymethyl cellulose acetate blend ultrafiltration membranes. Desalination *311*, 80–89.

Han, X., Wang, Y., Cao, X., Dai, Y., Liu, Y., Dong, Z., Zhang, Z., and Liu, Y. (2019). Adsorptive performance of ship-type nano-cage polyoxometalates for U (VI) in aqueous solution. App Surf Sci. *484*, 1035–1040.

He, J., Sun, F., Han, F., Gu, J., Ou, M., Xu, W., and Xu, X. (2018). Preparation of a novel polyacrylic acid and chitosan interpenetrating network hydrogel for removal of U (VI) from aqueous solutions. RSC Adv. *8*, 12684–12691.

Hu, R., Ren, X., Hou, G., Shao, D., Gong, Y., Chen, X., Tan, X., Wang, X., and Nagatsu, M. (2016). A carboxymethyl cellulose modified magnetic bentonite composite for efficient enrichment of radionuclides. RSC Adv. *6*, 65136–65145.

Huo, J., Marcello, M., Garai, A., and Bradshaw, D. (2013). MOF-polymer composite microcapsules derived from pickering emulsions. Adv. Mater. *25*, 2717–2722.

Jahan, M., Liu, Z., and Loh, K.P. (2013). A Graphene oxide and copper-centered metal organic framework composite as a tri-functional catalyst for HER, OER, and ORR. Adv. Funct. Mater. *23*, 5363–5372.

Jasuja, H., Huang, Y.G., and Walton, K.S. (2012). Adjusting the stability of metal–organic frameworks under humid conditions by ligand functionalization. Langmuir *28*, 16874–16880.

Kalaj, M., Bentz, K.C., Ayala, S., Jr., Palomba, J.M., Barcus, K.S., Katayama, Y., and Cohen, S.M. (2020). MOF-polymer hybrid materials: from simple composites to tailored architectures. Chem. Rev. *120*, 8267–8302.

Kou, J., and Sun, L.B. (2018). Fabrication of metal–organic frameworks inside silica nanopores with significantly enhanced hydrostability and catalytic activity. ACS Appl. Mater. Inter. *10*, 12051–12059.

Kushwaha, S., Mane, M., Ravindranathan, S., and Das, A. (2020). Polymer nanorings with uranium specific clefts for selective recovery of uranium from acidic effluents via reductive adsorption. ACS Sensors *5*, 3254–3263.

Li, J.Q., Feng, X.F., Zhang, L., Wu, H.Q., Yan, C.S., Xiong, Y.Y., Gao, H.Y., and Luo, F. (2017). Direct extraction of U (VI) from alkaline solution and seawater via anion exchange by metal-organic framework. Chem. Eng. J. *316*, 154–159.

Li, L., Ma, W., Shen, S., Huang, H., Bai, Y., and Liu, H. (2016). A combined experimental and theoretical study on the extraction of uranium by amino-derived metal–organic frameworks through post-synthetic strategy. ACS Appl. Mater. Inter. *8*, 31032–31041.

Li, R., Tong, J., Zhang, G., Gao, M., Cai, D., and Wu, Z. (2018). Improving the combustion efficiency of diesel fuel and lowering PM2. 5 using palygorskite-based nanocomposite and removing Cd^{2+} by the residue. Appl. Clay Sci. *162*, 276–287.

Li, Z., Xiao, J., Chen, C., Zhao, L., Wu, Z., Liu, L., and Cai, D. (2020). Promoting desert biocrust formation using aquatic cyanobacteria with the aid of MOF-based nanocomposite. Sci. Total Environ. *708*, 134824.

Liu, R., Zhang, W., Chen, Y., and Wang, Y. (2020). Uranium (VI) adsorption by copper and copper/iron bimetallic central MOFs. Colloid Surf. A *587*, 124334.

Lv, Z., Wang, H., Chen, C., Yang, S., Chen, L., Alsaedi, A., and Hayat, T. (2019). Enhanced removal of uranium (VI) from aqueous solution by a novel Mg-MOF-74-derived porous MgO/carbon adsorbent. J. Colloid Interf. Sci. *537*, A1–A10.

Mei, L., Li, F.Z., Lan, J.H., Wang, C.Z., Xu, C., Deng, H., Wu, Q.Y., Hu, K.Q., Wang, L., and Chai, Z.F. (2019). Anion-adaptive crystalline cationic material for $^{99}TcO_4^-$ trapping. Nat. Commun. *10*, 1–12.

Ouyang, J., Liu, Z., Zhang, L., Wang, Y., and Zhou, L. (2020). Analysis of influencing factors of heavy metals pollution in farmland-rice system around a uranium tailings dam. Process. Saf. Environ. *139*, 124–132.

Saadiah, M., Zhang, D., Nagao, Y., Muzakir, S., and Samsudin, A. (2019). Reducing crystallinity on thin film based CMC/PVA hybrid polymer for application as a host in polymer electrolytes. J. Non-cryst Sol. *511*, 201–211.

Takigami, M., Amada, H., Nagasawa, N., Yagi, T., Kasahara, T., Takigami, S., and Tamada, M. (2007). Preparation and properties of CMC gel. Trans. Mater. Res. Soc. Jpn. *32*, 713–716.

Tang, N., Liang, J., Niu, C., Wang, H., Luo, Y., Xing, W., Ye, S., Liang, C., Guo, H., and Guo, J. (2020). Amidoxime-based materials for uranium recovery and removal. J. Mater. Chem. A. *8*, 7588–7625.

Tang, Y., Zhang, H., Liu, X., Cai, D., Feng, H., Miao, C., Wang, X., Wu, Z., and Yu, Z. (2011). Flocculation of harmful algal blooms by modified attapulgite and its safety evaluation. Water Res. *45*, 2855–2862.

Thi, Q.V., Nguyen, N.Q., Oh, I., Hong, J., Koo, C.M., Tung, N.T., and Sohn, D. (2021). Thorny trunk-like structure of reduced graphene oxide/HKUST-1 MOF for enhanced EMI shielding capability. Ceram. Int. *47*, 10027–10034.

Wang, L., Yuan, L., Chen, K., Zhang, Y., Deng, Q., Du, S., Huang, Q., Zheng, L., Zhang, J., and Chai, Z. (2016). Loading actinides in multilayered structures for nuclear waste treatment: the first case study of uranium capture with vanadium carbide MXene. ACS Appl. Mater. Inter. *8*, 16396–16403.

Wang, Z., Meng, Q., Ma, R., Wang, Z., Yang, Y., Sha, H., Ma, X., Ruan, X., Zou, X., and Yuan, Y. (2020). Constructing an ion pathway for uranium extraction from seawater. Chem *6*, 1683–1691.

Wei, C., Yang, M., Guo, Y., Xu, W., Gu, J., Ou, M., and Xu, X. (2018). Highly efficient removal of uranium (VI) from aqueous solutions by poly (acrylic acid-co-acrylamide) hydrogels. J. Radioanal. Nucl. Chem. *315*, 211–221.

Wu, Y., Pang, H., Yao, W., Wang, X., Yu, S., Yu, Z., and Wang, X. (2018). Synthesis of rod-like metal-organic framework (MOF-5) nanomaterial for efficient removal of U (VI): batch experiments and spectroscopy study. Sci. Bull *63*, 831–839.

Xiao, J., Zhang, G., Qian, J., Sun, X., Tian, J., Zhong, K., Cai, D., and Wu, Z. (2018). Fabricating high-performance T-2-weighted contrast agents via adjusting composition and size of nanomagnetic iron oxide. ACS Appl. Mater. Inter. *10*, 7003–7011.

Xiong, X.H., Tao, Y., Yu, Z.W., Yang, L.X., Sun, L.J., Fan, Y.L., and Luo, F. (2020). Selective extraction of thorium from uranium and rare earth elements using sulfonated covalent organic framework and its membrane derivate. Chem. Eng. J. *384*, 123240.

Yang, W., Bai, Z.Q., Shi, W.Q., Yuan, L.Y., Tian, T., Chai, Z.F., Wang, H., and Sun, Z.M. (2013). MOF-76: from a luminescent probe to highly efficient U VI sorption material. Chem. Commun. *49*, 10415–10417.

Yang, W., Pan, Q., Song, S., and Zhang, H. (2019). Metal–organic framework-based materials for the recovery of uranium from aqueous solutions. Inorg. Chem. Front *6*, 1924–1937.

Yi, X., Xu, Z., Liu, Y., Guo, X., Ou, M., and Xu, X. (2017). Highly efficient removal of uranium (VI) from wastewater by polyacrylic acid hydrogels. RSC Adv. *7*, 6278–6287.

Yuan, L.Y., Gao, G., Feng, C.Q., Chai, Z.F., and Shi, W.Q. (2020). A new family of actinide sorbents with more open porous structure: fibrous functionalized silica microspheres. Chem. Eng. J. *385*, 123892.

Yuan, L.Y., Liu, Y.L., Shi, W.Q., Lv, Y.L., Lan, J.H., Zhao, Y.L., and Chai, Z.F. (2011). High performance of phosphonate-functionalized mesoporous silica for U (VI) sorption from aqueous solution. Dalton T *40*, 7446–7453.

Zhang, N., Yuan, L.Y., Guo, W.L., Luo, S.Z., Chai, Z.F., and Shi, W.-Q. (2017). Extending the use of highly porous and functionalized MOFs to Th (IV) capture. ACS Appl. Mater. Inter. *9*, 25216–25224.

Zhu, L., Sheng, D., Xu, C., Dai, X., Silver, M.A., Li, J., Li, P., Wang, Y., Wang, Y., and Chen, L. (2017). Identifying the recognition site for selective trapping of 99TcO4–in a hydrolytically stable and radiation resistant cationic metal–organic framework. J. Am. Chem. Soc. *139*, 14873–14876.

Zou, D.L., He, L.L., Xiao, D.W., Zhao, Y.W., Qiu, Z.C., Chao, L., and Fan, L. (2020). Microstructure and mechanical properties of fine grained uranium prepared by ECAP and subsequent intermediate heat treatment. T Nonferr Metal Soc. *30*, 2749–2756.

STAR★METHODS

KEY RESOURCES TABLE

REAGENT or RESOURCE	SOURCE	IDENTIFIER
Chemicals, peptides, and recombinant proteins		
Copper nitrate trihydrate	Sinopharm Chemical Reagent Co., Ltd.,	CAS:10031-43-3
1,3,5-Benzenetricarboxylic acid	Alfa Aesar Chemical Co., Ltd.,	CAS: 554-95-0
Ethanol	Xilong Chemical Reagent Co., Ltd.;	CAS: 64-17-5
Acetone	Beijing Chemical Reagent	CAS: 67-64-1
N,N-Dimethylformamide	Beijing Chemical Reagent	CAS: 68-12-2
Polyvinyl alcohol 0588	Aladdin Reagent Co., Ltd.,	CAS: 9002-89-5
Sodium carboxymethyl cellulose	Sinopharm Chemical Reagent Co., Ltd.,	CAS: 9004-32-4
Calcium chloride	Sinopharm Chemical Reagent Co., Ltd.,	CAS: 10043-52-4
Other		
Power X-ray diffractometer	Bruker D8 Advance diffractometer,	https://www.bruker.com/zh/products-and-solutions/diffractometers-and-scattering-systems/x-ray-diffractometers/d8-advance-family/d8-advance-eco.html
Fourier transform infrared spectrum	Bruker Tensor 27 spectrometer	https://www.antpedia.com/instrument/235/
Nitrogen adsorption and desorption apparatus	Micromeritics ASAP 2020	https://www.micromeritics.com/asap-2020-plus/
Field emission scanning electron microscope	Zeiss Gemini Sigma 300 VP SEM	https://ner.ecut.edu.cn/5b/dc/c1125a89052/page.htm
Thermogravimetric analyzer	Instruments Q500	https://camcor.uoregon.edu/equipment/ta-instruments-thermogravimetric-analyzer-tga-q500/
Spring Tension and Compression Testing Machine	Jinan Hongtuo Testing Technology Co., Ltd., WDT-5	https://m.makepolo.com/product/100008089688.html
Inductively coupled plasma optical emission spectroscopy	Horiba JY 2000-2	https://www.instrument.com.cn/netshow/C199672.htm

RESOURCE AVAILABILITY

Lead contact

Further information and requests for resources should be directed to and will be fulfilled by the lead contact, Weiqun Shi (shiwq@ihep.ac.cn).

Material availability

This study did not generate new unique reagents.

Data and code availability

- All data reported in this article will be shared by the lead contact upon request.
- This study does not report original code.
- Any additional information required to reanalyze the data reported in this paper is available from the lead contact upon request.

METHODS DETAILS

MOF synthesis

HKUST-1 crystals were synthesized by hydrothermal method (Thi et al., 2021). Specifically, a solution of $Cu(NO_3)_2 \cdot 6H_2O$ (0.88 g, 3.64 mmol) in deionized water (12 mL) was added to a solution of H_3BTC (0.42 g, 2.00 mmol) in ethanol (12 mL) and set to stir at room temperature for 1 h. Then the mixture was

transferred to a teflon autoclave lined and reacted in an oven at 120°C for 24 h. After being naturally cooled to room temperature, blue powders from the mixture was obtained by filtration, followed by washing several times with deionized water and ethanol. Finally, the crystals were dried at 120°C for 16 h and then stored in an oven at 60°C for later use.

Composites synthesis

The composites with different mass ratios of 20, 50 and 80 wt% (w/w) were synthesized by using MOF/CMC weight ratios of 200/800, 500/500 and 800/200 mg, respectively (Chen et al., 2016a, 2016b). First, a certain amount of HKUST-1 powder was disperse in 10 mL DMF/acetone (v/v = 2/3) solution, followed by 20 min ultrasonic treatment. After rotary evaporation to remove acetone, 6 mL deionized water was added, followed by another 20 min sonication. Then, the mixture was transferred to the pre-prepared CMC solution (dissolve the quantitative CMC in 10 mL deionized water). After stirring for 4 h, the target composites were obtained by freeze-drying, which are denoted as 20 wt% HK@CMC, 50 wt% HK@CMC, 80 wt% HK@CMC, respectively.

Preparation of derivative film

A solution of 5 wt% polyvinyl alcohol (PVA) solution (1.0 g) was added to CMC solution containing 200 mg in 10 mL deionized water, followed by stirring at room temperature for 1 h. Then a solution containing 750 mg HKUST-1 was transferred to the CMC/PVA solution, and was stirred to mix well. A certain amount of the mixed solution was transferred to a petri dish. After adding 1 mL of 5 wt% $CaCl_2$-ethanol solution for 5 min cross-linking, a derivative film was then obtained by vacuum filter.

Static adsorption experiments

In a typical adsorption experiment, 5 mg of adsorbent was added into 10 mL of U(VI) solution of a certain concentration, and the pH was adjusted using 0.1 mol L^{-1} NaOH and 0.1 mol L^{-1} HCl. Stirring for 6 h at room temperature. Then, the supernatants were collected using poly (ether sulfone) syringe filters and diluted with 5 wt % HNO_3 before determination of U(VI) concentration. The concentrations of U(VI) in the aqueous solution were determined by the inductively coupled plasma optical emission spectroscopy (ICP-OES). The adsorption capacity (q_e) of U(VI) are defined as follows:

$$q_e = \frac{(C_0 - C_e) \times V}{m} \quad \text{(Equation 1)}$$

where q_e (mg g^{-1}) is the adsorption capacity of the adsorbent; C_0 (mg L^{-1}) and C_e (mg L^{-1}) are initial and final concentrations of U(VI), respectively; V (L) is the volume of the U(VI) solution taken; m (g) is the mass of the adsorbent. All the values were measured in duplicate with the uncertainty within 5%.

Dynamic adsorption experiments

The dynamic adsorption experiment was carried out in a vacuum pumping device (Figure S1). 5 mL of 10 mg L^{-1} U(VI) solution was added to the filter cup and a vacuum water circulation pump was used to provide negative pressure for filtration. The pressure of the suction filter was adjusted to 0.01 MPa through the three-way valve (connected to the three-way valve), and the separation experiment was conducted. The calculation formula for the removal percentage (R%) and desorption percentage (D%) of U(VI) are as follows:

$$R(\%) = \frac{C_0 - C_e}{C_0} \times 100\% \quad \text{(Equation 2)}$$

$$D(\%) = \frac{C_D \times V_D}{C_0 \times V_0} \times 100\% \quad \text{(Equation 3)}$$

where C_D (mg L^{-1}) and V_D (L) are the concentrations of U(VI) in the filtrate and the amount of eluent, respectively.

The adsorption data fitting by kinetics models

The pseudo-first-order and pseudo-second-order kinetic models were applied to analyze the experimentally observed kinetic data. The expressions of the two models are as follows:

$$\ln(q_e - q_t) = \ln q_e - k_1 t \quad \text{(Equation 4)}$$

$$\frac{t}{q_t} = \frac{1}{k_2 q_e^2} + \frac{t}{q_e} \quad \text{(Equation 5)}$$

where q_e (mg g^{-1}) and q_t (mg g^{-1}) are the amounts of U(VI) ions adsorbed in the composites at equilibrium and at time of t (min), respectively; k_1 (min^{-1}) and k_2 (g mg^{-1} min^{-1}) are the pseudo-first-order and pseudo-second-order kinetic adsorption rate constants, respectively.

The adsorption data fitting by isotherm models

The Langmuir model assumes that the adsorption of metal ions occurs on a uniform surface by a single layer of adsorption, while the Freundlich equation is an empirical formula that assumes adsorption on a non-uniform surface. The functional expressions of Langmuir model and Freundlich model are described as follows:

$$\frac{C_e}{q_e} = \frac{C_e}{q_m} + \frac{1}{K_L q_m} \quad \text{(Equation 6)}$$

$$\ln q_e = \ln K_F + \frac{1}{n} \ln C_e \quad \text{(Equation 7)}$$

where C_e (mg L^{-1}) is the equilibrium concentration of U(VI) ions; q_e (mg g^{-1}) and q_m (mg g^{-1}) are the equilibrium adsorption amount and the saturated adsorption amount of U(VI) ions, respectively; K_L (L mg^{-1}) is an equilibrium constant related to the binding strength; n and K_F (L mg^{-1}) are Freundlich constants which are indicators of the adsorption capacity and adsorption intensity, respectively.

Selective adsorption of U(VI) by the composites

The distribution coefficient (K_d) and selectivity coefficient ($S_{U/M}$) for U(VI) relative to competing ions is defined as:

$$K_d = \frac{q_e}{C_e} \times 1000 \quad \text{(Equation 8)}$$

$$S = \frac{K_d^U}{K_d^M} \quad \text{(Equation 9)}$$

where C_e (mg L^{-1}) is the concentration of ions in adsorption equilibrium; q_e (mg g^{-1}) is the adsorption amount in equilibrium; $K_d^{U(VI)}$ and K_d^M are the partition coefficients of U(VI) and metal ions in the adsorbent and solution, respectively.